

Quantitative Evaluation of Cellular Uptake and Trafficking of Plain and Polyethylene Glycol-Coated Gold Nanoparticles

Christina Brandenberger, Christian Mühlfeld, Zulqurnain Ali, Anke-Gabriele Lenz, Otmar Schmid, Wolfgang J. Parak, Peter Gehr, and Barbara Rothen-Rutishauser*

This study addresses the cellular uptake and intracellular trafficking of 15-nm gold nanoparticles (NPs), either plain (i.e., stabilized with citrate) or coated with polyethylene glycol (PEG), exposed to human alveolar epithelial cells (A549) at the air–liquid interface for 1, 4, and 24 h. Quantitative analysis by stereology on transmission electron microscopy images reveals a significant, nonrandom intracellular distribution for both NP types. No particles are observed in the nucleus, mitochondria, endoplasmic reticulum, or golgi. The cytosol is not a preferred cellular compartment for both NP types, although significantly more PEG-coated than citrate-stabilized NPs are present there. The preferred particle localizations are vesicles of different sizes (<150, 150–1000, >1000 nm). This is observed for both NP types and indicates a predominant uptake by endocytosis. Subsequent inhibition of caveolin- and clathrin-mediated endocytosis by methyl- β -cyclodextrin ($M\beta$ CD) results in a significant reduction of intracellular NPs. The inhibition, however, is more pronounced for PEG-coated than citrate-stabilized NPs. The latter are mostly found in larger vesicles; therefore, they are potentially taken up by macropinocytosis, which is not inhibited by $M\beta$ CD. With prolonged exposure times, both NPs are preferentially localized in larger-sized intracellular vesicles such as lysosomes, thus indicating intracellular particle trafficking. This quantitative evaluation reveals that NP surface coatings modulate endocytotic uptake pathways and cellular NP trafficking. Other nonendocytotic entry mechanisms are found to be involved as well, as indicated by localization of a minority of PEG-coated NPs in the cytosol.

Keywords:

- cells
- coatings
- gold
- nanoparticles
- stereology

[*] Dr. B. Rothen-Rutishauser, Dr. C. Brandenberger, Prof. P. Gehr
 Institute of Anatomy
 University of Bern
 Bern 3012 (Switzerland)
 E-mail: rothen@ana.unibe.ch
 Dr. C. Mühlfeld
 Institute of Anatomy and Cell Biology
 Justus-Liebig-University Giessen
 Giessen 35385 (Germany)

Z. Ali, Prof. W. J. Parak
 Fachbereich Physik
 Philipps Universität Marburg
 Marburg 35032 (Germany)
 Dr. A.-G. Lenz, Prof. O. Schmid
 Comprehensive Pneumology Center
 Institute of Lung Biology and Disease
 Helmholtz Zentrum München
 Neuherberg 85764 (Germany)

Supporting Information is available on the WWW under <http://www.small-journal.com> or from the author.

DOI: 10.1002/sml.201000528

1. Introduction

Nanoparticles (NPs; <100 nm in all three dimensions, ISO/TS 27687:2008) show promising features for pharmaceutical applications,^[1,2] especially for targeted drug delivery,^[3,4] biomedical imaging,^[5] or biosensing.^[6] However, biomedical applications require a detailed understanding of interactions between NPs and biological systems. Upon exposure, NPs may interact with cells and enter them by different mechanisms dependent on their size, material, and surface characteristics.^[7] The pathways of entry and the subsequent intracellular particle distribution influence the biological effects caused by particles.^[8] To understand a possible relationship between intracellular distribution and induced effects, it is important to investigate the processes involved in cellular uptake of NPs and their intracellular trafficking.

Quantitative uptake studies with different well-characterized NPs indicate that size, shape, surface charge, and coating modify the amount of cellular particle uptake.^[9–12] The mechanisms by which particles of different physical and chemical properties enter the cells has also been the subject of diverse investigations, and there is convincing evidence that different mechanisms are involved, such as phagocytosis, macropinocytosis, clathrin-mediated endocytosis, caveolae-mediated endocytosis, and direct entering mechanisms summarized by the term adhesive interactions (reviewed in References [7,13,14]). Besides quantitative and mechanistic uptake studies, there are reports on intracellular particle localizations. Most frequently, NPs have been reported to be found in intracellular vesicles including early and late endosomes, lysosomes, or phagosomes.^[15,16] Some studies also report the presence of NPs in the cytosol,^[17–19] in mitochondria,^[20] and in the nucleus.^[18,21] However, so far no quantitative study on relative intracellular particle localization has been performed, with regard to the number of particles associated with intracellular compartments relative to their size. Therefore this study aimed to quantify the relative intracellular distribution of gold NPs over time.

Gold NPs have a broad spectrum of applications in nanomedicine^[22] as they are supposedly nontoxic,^[23] suitable for biomedical imaging,^[5] and they can be coated with medical substrates.^[24] Coatings with polyethylene glycol (PEG) are quite often used in nanomedical applications since this material is biocompatible, stabilizes the particles, and reduces their reactivity.^[25] Furthermore, it has been shown that PEG coatings can decrease the toxicity of potentially harmful NP materials and simplify particle engineering.^[26] However, it is known that surface coatings modify targeting^[27] and cellular uptake of gold NPs.^[28] For this reason, the study also aimed to compare uptake mechanisms and intracellular trafficking of gold NPs, either coated with PEG or plain (i.e., stabilized in citrate buffer). The gold NPs had a core 15 nm in diameter, since different studies have used similar-sized gold NPs as carriers for drugs or DNA.^[3,24,29] In addition, these particles were easily detectable by transmission electron microscopy (TEM) within the cells.

The particles were deposited onto human alveolar epithelial cells (A549 cell line) at the air–liquid interface of the cell culture, by using a recently developed cell exposure

system.^[30] This system has many advantages compared to suspension experiments. Air–liquid interface cell exposure (ALICE) mimics the physiological conditions of aerosol inhalation in the lungs more realistically and offers a beneficial system for pharmacological and toxicological *in vitro* studies. The human A549 lung cell line used in this study is well established and can be cultured at the air–liquid interface. After a few hours of maintenance at the air–liquid interface, the cells start producing and secreting surfactant, thus lowering the surface tension and providing a similar microenvironment to that found in pulmonary alveoli.^[31] In addition, the ALICE system allows an exact dosimetry and minimizes inadvertent particle effects such as agglomeration and diffusional loss, as it occurs under submerged exposure conditions.^[32] Following NP deposition, the cells were exposed to the particles for 1, 4, and 24 h, which allowed the analysis of intracellular NP distribution over time. Since different endocytotic uptake mechanisms were assumed to be involved in cellular NP entry, partial inhibition of endocytotic pathways, such as caveolin- and clathrin-mediated endocytosis, was induced by methyl- β -cyclodextrin (M β CD).^[33] For analyzes of intracellular NP distribution, the cells were fixed and processed for TEM. The compartmental localization of the NPs was determined relative to the size of the intracellular compartment by the method of the relative deposition index (RDI).^[34] This approach is based on the principles of stereology and enables the identification of preferentially occupied cell compartments as well as the intracellular trafficking of gold NPs.

2. Results

2.1. Relative Particle Distribution within the Cells

The relative intracellular particle distribution of 15-nm gold NPs, plain (i.e., citrate-stabilized) and PEG-coated, was evaluated after particle exposure times of 1, 4, and 24 h by means of stereology on TEM images. The cell compartments that were included in the study were intracellular vesicles, cytoplasm, nucleus, mitochondria, endoplasmic reticulum (ER) or golgi, and residual, defined as the locations that could not be assigned to one of the other compartments. A functional vesicle categorization on the TEM level could not be used for a quantitative approach, due to difficulties in specifically marking all intracellular vesicles. Therefore, we used size-dependent categories (<150, 150–1000, >1000 nm) referring to the size of primary endocytotic vesicles (<150 nm), medium-sized vesicles (between 150 and 1000 nm) such as endosomes or multi-vesicular bodies, and larger-sized vesicles (>1000 nm) such as phagosomes or lysosomes.^[35]

Both plain and PEG-coated NPs were found in vesicles of different sizes (Figure 1A and B), in residual compartments (data not shown), or in the cytoplasm (Figure 1B). With the quantitative analysis described in the Experimental Section, RDI and χ^2 values were obtained for each experimental setting. An RDI > 1 indicates a preferentially populated compartment, that is, more NPs were found than expected for random intracellular NP distribution; an RDI < 1 represents a compartment that contains fewer NPs than expected solely from its size. Using the χ^2 test, it was statistically analyzed whether the

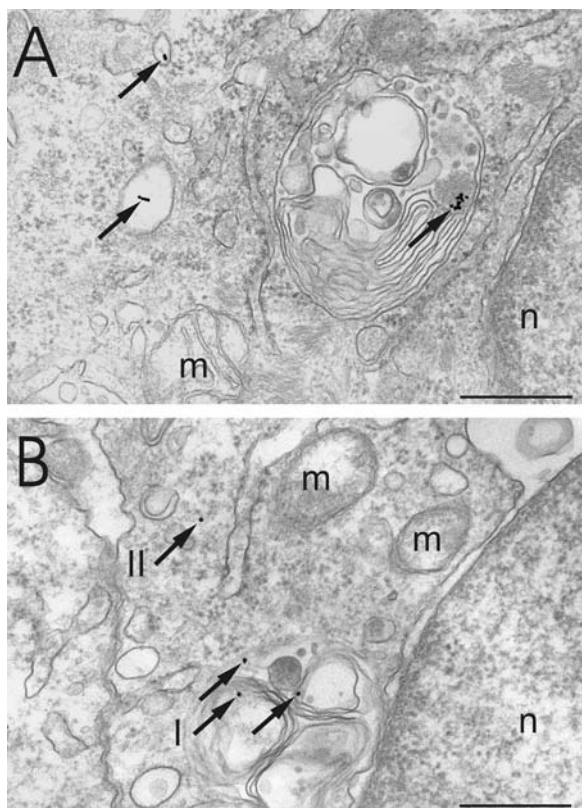


Figure 1. Intracellular compartments where particles were encountered with A) plain gold NPs and B) PEG-coated gold NPs. In (A), the particles (see arrows) are localized within vesicles of different size categories (<150, 150–1000, >1000 nm) and in (B) within a lysosome (arrows I) and in the cytosol (arrow II). n = nucleus, m = mitochondria; scale bars: 500 nm.

particles were equally distributed within the compartments. An example of how the calculations were performed, including the results of intracellular distribution for plain NPs with 1 h exposure time, can be found in the Supporting Information. The total RDI values of all compartments and incubation time points of plain and PEG-coated NPs are shown in Figure 2. Statistical analysis revealed a significant ($p < 0.05$), nonrandom distribution of plain and PEG-coated NPs in the cells. Preferentially targeted compartments (RDI > 1) were vesicles of all sizes, whereas all other compartments such as residuals and cytoplasm showed an RDI < 1. No particles were encountered in the nucleus, mitochondria, and ER or golgi. Table 1 summarizes the RDI and χ^2 values of all compartments and experimental time points.

A further comparison between the relative number of events of plain and PEG-coated NPs and the temporal development of the particle distribution within the cells was statistically analyzed with the χ^2 test (Figure 3A). The plain gold NPs showed no significant change of particle distribution between 1 and 4 h, but a major shift of particles localized in the smallest vesicle fraction (<150 nm) towards the largest (>1000 nm) occurred between 4 and 24 h. A major shift was also observed for the PEG-coated NPs both between 1 and 4 h and also between 4 and 24 h. The middle-sized vesicle fraction (150–1000 nm) remained almost constant over time for both NP

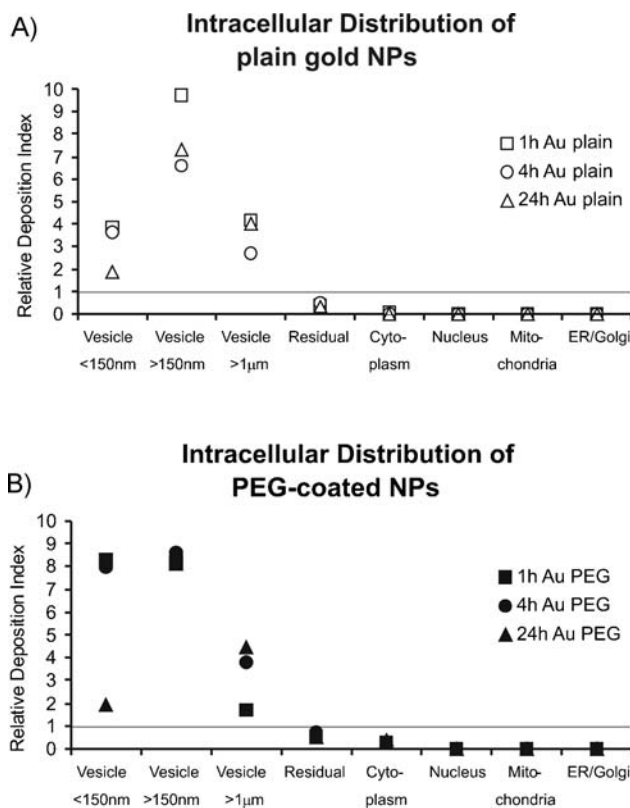


Figure 2. Intracellular particle distribution of A) plain gold (Au) NPs and B) PEG-coated Au NPs after 1, 4, and 24 h post-exposure incubation time. Both particle types showed a significant nonrandom distribution ($p < 0.05$) within the cells with a preference for intracellular vesicles of all three sizes (RDI > 1). A minor fraction of NPs (RDI < 1) was localized in the cytosol and in residual compartments, which could not be assigned to any of the other compartments. No particles were found in the nucleus, mitochondria, and ER/golgi.

types. A comparison between PEG-coated and plain particles is shown in Figure 3B. The distribution of the two NP types after 1 h exposure time differed within all three vesicle sizes and the cytoplasm. However, after 4 and 24 h significantly more plain NPs were localized in the middle-sized vesicle fraction and more PEG-coated NPs were located in the cytoplasm.

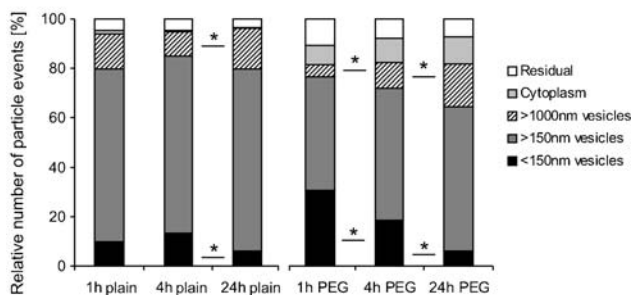
2.2. Effects of NP Agglomerates on Uptake and Intracellular Distribution

The largest diameter (henceforth referred to as size) of each particle event (either single NP or agglomerate) was measured and the particle size distribution of single particles and agglomerates was evaluated in terms of the size frequency and how this affected intracellular particle distribution. The relative frequency of agglomerate sizes shows different intracellular agglomeration behavior between the two particle types (see the Supporting Information). At least 94% of the PEG-coated NPs remained as single particles at all time points and no agglomerates >100 nm were detected, whereas an increasing intracellular agglomeration with time was observed for plain NPs: 22% of agglomerates of plain NPs were in the size range of >100 nm in diameter after 1 h incubation time and this

Table 1. RDI and χ^2 test values of all compartments at incubation times of 1, 4, and 24 h for plain NPs (A) and PEG-coated NPs (B).

A: Cell compartments	1 h RDI	1 h χ^2	4 h RDI	4 h χ^2	24 h RDI	24 h χ^2
vesicle <150 nm	3.83	111	3.61	115	1.87	10
vesicle >150 nm	9.71	2882	6.62	1545	7.29	1703
vesicle >1000 nm	4.19	187	2.69	48	4	155
ER/golgi	0	20	0	14	0	14
cytoplasm	0.03	171	0.01	160	0.01	156
nucleus	0	176	0	135	0	119
mitochondria	0	20	0	15	0	15
residual	0.41	21	0.49	12	0.34	19
Total	18.17	3588	13.42	2044	13.51	2191
B: Cell compartments	1 h PEG RDI	1 h PEG χ^2	4 h PEG RDI	4 h PEG χ^2	24 h PEG RDI	24 h PEG χ^2
vesicle <150 nm	8.30	578	7.98	482	1.91	11
vesicle >150 nm	8.20	848	8.60	1499	8.11	1583
vesicle >1000 nm	1.72	4	3.79	92	4.46	204
ER/golgi	0	11	0	14	0	19
cytoplasm	0.30	37	0.27	84	0.39	45
nucleus	0	109	0	142	0	152
mitochondria	0	14	0	16	0	18
residual	0.53	13	0.71	4	0.50	16
Total	19.05	1614	21.35	2333	15.37	2048

A) Time Dependent Particle Distribution



B) Coating Dependent Particle Distribution

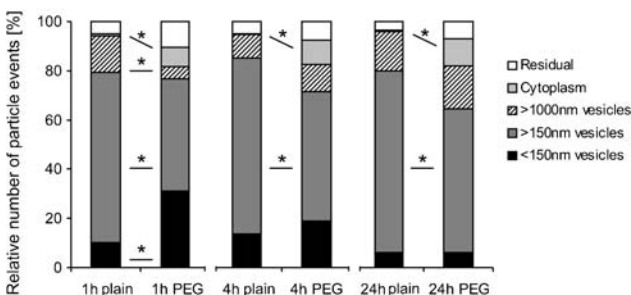


Figure 3. A) Time- and B) coating-dependent intracellular distribution of gold NPs. The time-dependent intracellular distribution (A) of plain NPs revealed a significant ($p < 0.05$) difference between 4 and 24 h, which resulted in a decrease of the smallest vesicle fraction (<150 nm) and an increase in the largest vesicle fraction (>1000 nm). The same shift from smallest towards largest vesicle fraction was observed between all time points for PEG-coated NPs. The surface-coating-dependent intracellular particle distribution (B) revealed a major increase of PEG-coated NPs localized in the cytoplasm and a decrease in the middle-sized vesicle fraction at all time points. There is also a reduced localization in the largest vesicle fraction and an increase in the smallest vesicle fraction of PEG-coated NPs at 1 h. (* = $\chi^2 \geq 10\%$ of total χ^2 value).

fraction increased to 27% after 4 h and to 39% after 24 h. Comparing the relative intracellular distribution of single NPs and small agglomerates (≤ 100 nm in diameter) with bigger agglomerates (>100 nm in diameter) within the different cellular compartments, it was confirmed that agglomerates >100 nm were predominantly localized in the middle- and larger-sized vesicles (data not shown).

Further experiments were performed to compare the effects of particle agglomeration and diffusion under submerged exposure conditions with those in the ALICE system. Plain particles were mainly present as single particles if suspended in 10 mM citrate buffer, whereas when dissolved in cell culture medium (RPMI 1640 without fetal calf serum) they formed large agglomerates (see Supporting Information). An exposure with particles suspended in cell culture medium, at the same particle number concentration as in the ALICE experiments, resulted in a significant reduction of particles per cell compared to particle uptake in the ALICE. After 4 h of NP exposure in suspension, only 527 (standard deviation (SD) 307) particles/cell were counted, whereas significantly more (i.e., 3575 (SD 689) particles cell⁻¹) could be estimated after using the ALICE system. An increased intracellular particle agglomeration was further observed after submerged exposure. In suspension experiments, only 10.2% single NPs and 36.7% small agglomerates <100 nm were found to be intracellular, whereas in ALICE experiments 22.7% were present as single NPs and 73.2% as agglomerates <100 nm (see the Supporting Information). Hence, suspension experiments with plain NPs lead to an increased formation of agglomerates, which might influence particle uptake mechanisms, as well as a decrease in NP uptake rates due to diffusional NP loss in suspension.

2.3. Endocytosis Inhibition Study

NP-containing vesicles of different sizes were further analyzed qualitatively. As shown in Figure 4, particles were found in lysosomes (Figure 4A), caveosomes (Figure 4B), and

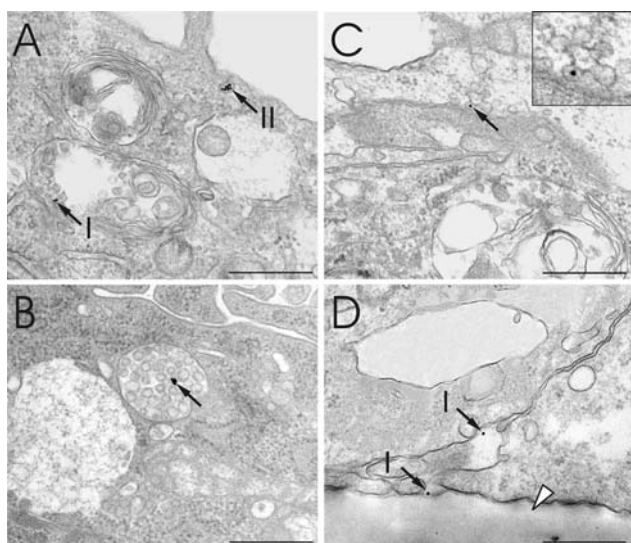


Figure 4. Different intracellular vesicles that can be identified by their morphology. These images are representative for both NP types. A) A small agglomerate of plain NPs in a lysosome (arrow I) and another one in a clathrin-coated pit (arrow II). B) A small particle agglomerate is localized in a multivesicular body (arrow). C) A single plain NP can be found in a caveosome (highlighted by an arrow and at a higher magnification in the inset). D) PEG-coated NPs are located in the intercellular space (black arrows I) at the basal side of the cells (white arrowhead points to the insert membrane on which cells are cultured). Most possibly, NPs have been translocated through the cells by transcytosis. Scale bars: 500 nm.

multivesicular bodies (Figure 4C). Invaginations of the apical plasma membrane, most possibly involved in the process of caveolin- or clathrin-mediated endocytosis (Figure 4A), as well as particle transcytosis through the cell (Figure 4D), were observed. These qualitative observations were confirmed for all time points and both NP types. The particle identification inside vesicular structures was assumed to result from endocytotic uptake processes and the different intracellular vesicles can also be related to specific endocytotic pathways (Figure 5). For this reason, partial inhibition of endocytosis was performed by cholesterol extraction with M β CD.^[28] The particle uptake as well as the intracellular distribution of particles was subsequently analyzed by stereological means after 1 and 4 h of incubation. Figure 6 shows the evaluation of the total number of particles taken up per cell. At 1 h, we found 362 (SD 184) compared to 2591 (SD 506) plain NPs taken up per cell with and without inhibition, respectively, and 15 (SD 6) compared to 526 (SD 61) PEG-coated NPs per cell with and without inhibition. At 4 h, the values were 1831 (SD 169) compared to 3575 (SD 689) with and without inhibition, respectively, for the plain NPs and 38 (SD 23) and 1068 (SD 424) for the PEG-coated NPs. Statistical analysis revealed a significantly enhanced uptake rate for plain NPs compared to PEG-coated NPs. This was observed in M β CD-treated and untreated cells. While particle uptake of plain gold NPs significantly increased after 4 h, uptake of PEG-coated NPs was still blocked at 4 h.

The RDI and intracellular distribution with and without inhibition were evaluated, but since the uptake of PEG-coated gold NPs was almost completely blocked, the number of counted intracellular particle events was too small to perform

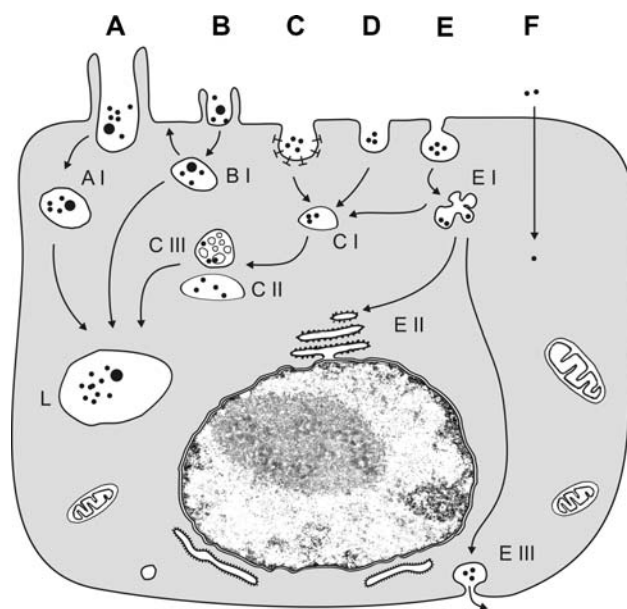


Figure 5. Cellular uptake mechanisms of NPs and related intracellular trafficking. A: Phagocytosis, occurring primarily in professional phagocytes, leading to phagosomes (AI) and phago-lysosomes (L). B: Macropinocytosis, engulfing NPs with poor selectivity, leading to macropinosomes (BI) which might be exocytosed or fused with lysosomes (L). C: Clathrin-mediated endocytosis, forming primary endosomes (CI) and late endosomes (CII) including multivesicular bodies (CIII). D: Clathrin- and caveolae-independent endocytotic pathways. E: Caveolae-mediated endocytosis, forming caveosomes (EI) which fuse with the ER (EII) or translocate through the cell (EIII). F: Particle diffusion/transport through the apical plasma membrane, resulting in particles located freely in the cytosol. The figure and descriptions are adapted from Mühlfeld et al. 2008^[39] and Hillaireau and Couvreur 2009,^[7] respectively.

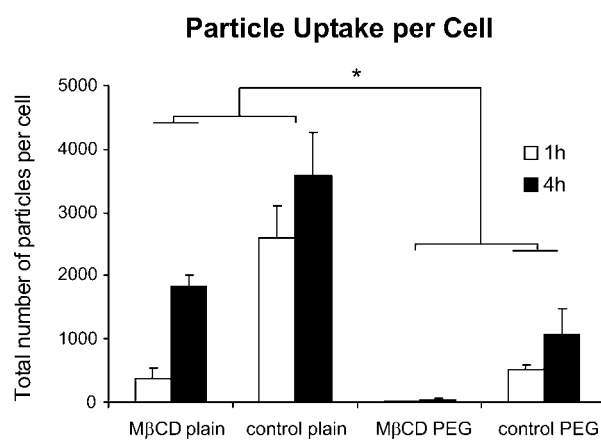


Figure 6. Cellular uptake of plain and PEG-coated NPs with and without inhibition of endocytosis by M β CD. The uptake of plain NPs was significantly increased compared to that of the PEG-coated NPs at both time points, with and without endocytotic inhibition. A significant increase between 1 and 4 h was further observed for plain NPs after endocytotic inhibition and PEG-coated NPs without inhibition. The inhibition resulted in a significantly reduced particle uptake for both particle types; however, it was stronger for PEG-coated NPs (86 and 49% reduction at 1 and 4 h, respectively, for the plain NPs and 97 and 96% reduction at 1 and 4 h, respectively, for the PEG-coated NPs). (* = $p < 0.05$).

statistics. However, the uptake of plain gold NPs was not entirely blocked and intracellular particle distribution was compared with the values without inhibition (Figure 7). A significantly different distribution was found in M β CD-treated cells compared to control cells at both time points. The inhibition resulted in an increase of particles localized in the largest vesicle fraction (>1000 nm), and a decrease in deposition in the middle- and smallest-sized vesicle fractions (<1000 nm).

3. Discussion

Within this study, we analyzed the uptake mechanisms and the intracellular trafficking of either plain (i.e., stabilized with citrate buffer) or PEG-coated (5 kD) 15-nm gold NPs. The particle exposure was performed at the air–liquid interface of cultured human alveolar epithelial cells (A549 cell line). This allowed an exact particle exposure dosimetry and enabled us to directly study and quantify particle–cell interactions. The spatial uniform dispersal of gold NPs onto the cells in the ALICE system was evaluated and diffusional particle loss or increased formation of agglomerates, as occurs under submerged exposure conditions,^[32] could be excluded (Supporting Information). Diverse previous studies investigating size- and coating-dependent particle uptake in submerged exposure conditions have not addressed this issue.^[9,11,36,37] However, this is of major importance since diffusional particle loss as well as increased particle agglomeration leads to a size-biased particle deposition which influences particle uptake mechanisms and rates.

The quantification of total particle uptake per cell was performed after 1 and 4 h of exposure, since particle uptake was shown to occur mainly within the first 4 h.^[23] The later time

point, 24 h, was only used to study subsequent intracellular NP distribution. The evaluation of NP uptake rates showed that significantly more plain NPs than PEG-coated NPs enter the cells. Although this was, in part, due to a slightly reduced deposition of the PEG-coated particles in the ALICE system ($16.1 \times 10^9 \pm 1.5 \times 10^9$ plain NPs cm^{-2} and $14.1 \times 10^9 \pm 1.6 \times 10^9$ PEG-coated NPs cm^{-2}), decreased uptake of PEG-coated NPs was still significant after correcting for the reduced deposition. The effect of decreased uptake of PEG-coated particles has also been shown previously.^[28] It is further known that PEG-coated particles can remain in the blood circulation for a longer time after intravenous injection, which also indicates reduced cellular uptake from circulation.^[38]

The intracellular NP distribution in relation to the relative intracellular compartment size was further assessed with a new quantitative approach, based on stereology, which allows the estimation of three-dimensional structures (number, length, surface, volume) from two-dimensional sections. This approach has been shown to be very beneficial for the intracellular quantification of NPs.^[19] However, further analysis with alternative detection methods, such as inductively coupled plasma mass spectrometry (ICP-MS), might also be valuable for a particular understanding of the mechanisms involved in NP uptake and trafficking.

We showed that both plain and PEG-coated 15-nm gold NPs were nonrandomly distributed in the cells, with preference for vesicles of all sizes (82–96% of both NP types). In accordance with other reports on intravesicular particle localization, it has been suggested that NP uptake by cells mainly occurs by endocytotic processes (reviewed in References [7,13,39]). Our findings also indicate that different endocytotic uptake mechanisms are responsible for the observed intravesicular particle localization, since both particle types were found in a variety of vesicular structures that are associated with different endocytotic pathways, such as clathrin- or caveolin-mediated endocytosis (e.g., caveosomes, clathrin-coated pits, multivesicular bodies, or particle transcytosis as shown in Figure 4). A functional characterization of all vesicle types for the quantitative evaluation was not possible on the TEM level. Therefore, vesicles were categorized by size into small-sized endocytotic vesicles (<150 nm), medium-sized vesicles (150–1000 nm) such as endosomes or multivesicular bodies, and larger-sized vesicles (>1000 nm) such as lysosomes or macropinosomes.^[35] It has to be noted that in two-dimensional image evaluation the true vesicle size is underestimated, and thus the categories cannot be interpreted as absolute values. However, since underestimation of vesicle size can be assumed to be equal in all experiments, a relative comparison within different experimental conditions is still possible.

The relative comparison within 1, 4, and 24 h exposure time revealed time-dependent particle localization in differently sized vesicles. A significant decrease of particles in the smallest vesicle fraction and an increase of particles in the largest fraction was found with time, thus inferring intracellular trafficking such as from primary endocytotic vesicles towards late endosomes and finally lysosomes^[7] (Figure 5). The effect was stronger for PEG-coated particles (significant

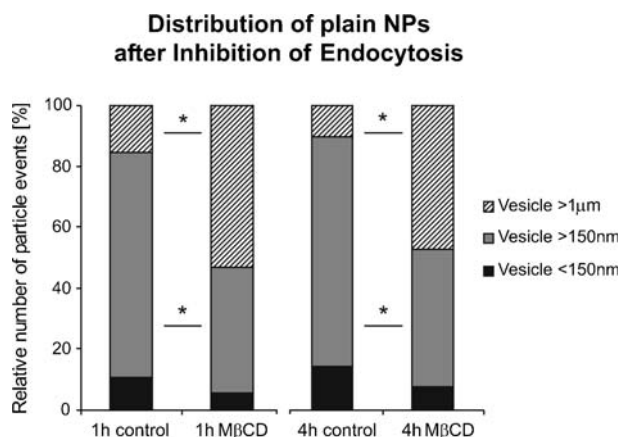


Figure 7. Effects on intracellular particle distribution after inhibition of endocytosis of plain gold NPs. While uptake of PEG-coated NPs was almost completely blocked and no statistics on intracellular distribution could therefore be performed, plain gold NPs were still taken up to a certain extent. However, intracellular particle distribution after M β CD inhibition was significantly different ($p < 0.05$) and resulted in a major particle localization in the largest vesicle fraction (>1000 nm), whereas particle deposition in the middle- and smallest-sized fractions (<1000 nm) was dramatically decreased. This might infer particle uptake via macropinocytosis, thus resulting in particle deposition in larger-sized vesicles compared to primary endocytotic vesicles as from clathrin- or caveolin-mediated endocytosis. (* = $\chi^2 \geq 10\%$ of total χ^2 value).

between 1, 4, and 24 h) than for the plain particles (significant between 4 and 24 h). This might be explained by the different agglomerate size of both particle types. The PEG-coated NPs mostly occurred as single particles in the cells whereas the plain NPs tended to form agglomerates, although they were initially shown to deposit homogeneously onto the cells (see Supporting Information). Regarding the cellular particle entry, it is therefore possible that larger agglomerates of plain particles are taken up by the cells via macropinocytosis, thus being localized in larger-sized vesicles such as macropinosomes after 1 h of exposure.

To further study endocytotic particle uptake and intracellular particle trafficking, we inhibited the endocytotic processes of caveolin- and clathrin-mediated endocytosis by cholesterol extraction via M β CD. Cholesterol extraction mainly acts on caveolin-mediated endocytosis, but was also shown to inhibit clathrin-mediated endocytosis.^[33] This inhibition resulted in a significant reduction of the number of particles per cell: 86 and 49% reduction at 1 and 4 h, respectively, for the plain particles and 97 and 96% reduction at 1 and 4 h, respectively, for the PEGylated particles. In particular, the PEG-coated NP uptake was almost completely blocked, which means that either caveolin- or clathrin-mediated endocytosis, or both pathways, are the main mechanisms of internalization for this NP type. We assume that caveolin-mediated endocytosis, which is known to be associated with transcytosis,^[35] is mainly involved in PEG-coated NP trafficking, since an increased number of PEGylated NPs were observed between cells or at the basal extracellular side (Figure 4D). The low number of intracellular PEG-coated NPs after inhibition did not allow any further statistical evaluation of their intracellular localization. However, it should be mentioned that not only the vesicular but also the cytosolic localization of PEG-coated NPs was relatively decreased. This implies that either endocytosis is involved in cytoplasmic particle transport or that the changes of apical plasma membrane composition due to cholesterol depletion further affected the cytosolic passage of PEG-coated NPs.

Since the uptake of plain gold NPs was less affected by the inhibition and resulted in a predominant localization in large vesicles, we assume that other uptake mechanisms are involved, such as macropinocytosis or phagocytosis as discussed before. When the total number of plain particles per cell was considered, 14.0 times fewer particles were found in the smallest vesicles, 12.9 times fewer in middle-sized vesicles, but only 2.1 times fewer particles in the largest vesicles of M β CD treated cells (at 1 h). This finding indicates that gold NP localization in the largest vesicle fraction was only marginally affected by M β CD treatment and plain intracellular NPs resulted from macropinocytotic uptake. This would be consistent with the observation of an increased number of plain NPs, localized in larger-sized vesicles such as macropinosomes after 1 h exposure time, compared to PEG-coated NPs as discussed before. Besides the different abilities to form agglomerates, we assume that the potential of protein binding to NPs was responsible for the different cellular uptake and the different distribution of citrate-stabilized and PEG-coated particles. Size, surface charge, and coatings of NPs have been shown to influence particle–protein interactions.^[40,41] These interactions might play a key role in the regulation of

endocytotic internalization pathways, since many different proteins are associated with a specific uptake mechanism.^[42] Plain gold NPs or other charged NPs show a broad spectrum of potential particle–protein interaction,^[43,44] whereas PEGylated particles were shown to interact with proteins to a lesser extent.^[45] Hence, reduced protein binding could explain the reduced cellular uptake of PEG-coated gold NPs.

A further interesting difference between plain and PEG-coated NPs was the NP localization in the cytosol. Although the cytosol was not the major target compartment (RDI < 1), there was a significantly increased number of PEG-coated NPs localized free in the cytosol compared with plain NPs. While the cytosolic presence of the plain particles can be considered to happen accidentally due to its very rare occurrence (RDI < <1), there seems to be a coating-dependent entry pathway to the cytosol for the PEGylated particles. It has previously been reported that PEG-coated particles have the potential to avoid vesicular trafficking and enter the cytosol.^[18] The possible explanation for their cytosolic uptake is that PEG can dissolve in both polar and nonpolar solvents, and has a high solubility in cell membranes.^[28] Therefore, a transmembrane passage of PEG-coated particles may be considered. However, the entry mechanism is not yet entirely understood and needs further investigation.

The other cellular compartments such as nucleus, mitochondria, or ER/golgi that were included in this study did not contain any NPs of either particle type. However, other reports found NPs to be localized in the nucleus^[18,21] or in mitochondria.^[20] Since their evaluation was not quantitative, it is possible that particles detected in these compartments might be the results of a single observation. Nevertheless, it has been shown that the surface coatings on the particles are responsible for intracellular targeting to cellular compartments, such as the cytosol^[17] and the nucleus.^[21] It is therefore not surprising that reports of particles entering the nucleus relate to NPs coated with nuclear tracer molecules.^[21] This observation could not be confirmed with the 15-nm gold NPs used in the current study; however, no NP coating with nuclear tracers was used.

4. Conclusions

The quantitative evaluation of the intracellular localization of NPs revealed that particle modifications such as PEGylation can influence particle agglomeration, cellular entry mechanisms, and intracellular trafficking. Plain and PEG-coated NPs were found to enter the cells by different endocytotic mechanisms and to be transported over time into larger-sized vesicles such as lysosomes, as described in Figure 5. Plain gold NPs were shown to be taken up by macropinocytosis as well as by clathrin- and caveolin-mediated endocytosis. This might be due to interactions with different proteins or lipids, related to one of the uptake mechanisms, and their increased ability to form agglomerates. The PEG-coated NPs were shown to enter the cells by caveolin- and/or clathrin-mediated endocytosis, but not by macropinocytosis. An increased transcytosis of PEG-coated NPs was further observed and a significant number of PEG-coated NPs were measured free within the cytosol. The

latter suggests an endocytosis-independent cellular entry mechanism. These findings show the influence of NP coatings, such as particle PEGylation, on cellular entry mechanisms and subsequent intracellular trafficking. This is of particular importance for the design of new pharmaceutical NPs and their targeting to specific intracellular locations. This study has also demonstrated that the ALICE system and stereological analysis are ideal tools for the evaluation of NP–cell interactions.

5. Experimental Section

Cell cultures: The A549 cell line was obtained from American Tissue Type Culture Collection (LGC Promochem, Molsheim, France). Cells from passage number 5 to 30 were maintained in RPMI 1640 medium (w/25 mM 4-(2-hydroxyethyl)-1-piperazine-ethanesulfonic acid (HEPES), Invitrogen, Karlsruhe, Germany) supplemented with 1% L-glutamine (Invitrogen, Germany), 1% penicillin/streptomycin (Biochrom, Berlin, Germany), and 10% fetal calf serum (FCS; Superior Biochrom, Berlin, Germany). The cells were seeded at a density of 0.5×10^6 cells mL⁻¹ on BD Falcon six-well plate cell culture transwell inserts (high-pore-density poly(ethylene terephthalate) (PET) membranes with a growth area of 4.2 cm² and 3.0 μm pore diameter; Omnilab GmbH, Munich, Germany). Inserts were placed in BD Falcon six-well tissue culture plates with 2 mL medium in the upper and 3 mL in the lower transwell chamber. The medium was changed twice a week. Cells were grown on transwell inserts under submerged conditions in medium for 7 days to grow to confluence. Twenty-four hours before exposure, the cells were exposed to the air–liquid interface^[31] and the medium in the lower chamber was replaced by fresh RPMI (1.8 mL) with supplements.

Particles: Commercially available plain 15-nm gold NPs stabilized with citrate buffer from British Biocell International (BBI; Plano GmbH, Wetzlar, Germany) were used in this study. The BBI gold suspension had a molar concentration of 2 nM. The molarity refers to the number of particles per mole and was determined by UV/Vis spectroscopy using the molecular extinction coefficient of their absorption at the plasmon peak: 3.64×10^8 m⁻¹cm⁻¹ as provided by BBI. In this study, exposures with a tenfold higher concentration (20 nM) were performed, which was reached for plain gold NPs by centrifugation of the original BBI solid suspension at 19 RCF (relative centrifugal force) for 20 min and removal of 90% of the citrate buffer. PEGylation of the particles was performed by ligand exchange: replacement of the citrate molecules on the surface of the gold NPs by thiolated PEG molecules due to the stronger and more stable bond between thiol groups and gold NPs. Thiolated PEG (SH-PEG_(5KD)-OCH₃, Rapp Polymere Company, Tübingen, Germany) was dissolved in Millipore water to make a stock solution with a molar concentration of 2 mM. A ratio of 50 PEG molecules per 1 nm² surface area of the gold NPs was used to mix the solution with the 2 nM colloidal gold suspension. The mixture was vigorously stirred with a magnetic stirring bar for 12 h. After the ligand exchange, the PEG-coated gold NP solution was rinsed three times with Millipore water with ultrafiltration (Viva Spin Ultrafiltration, 100 000

molecular weight cutoff (MWCO) PES, Sartorius Stedim, VS2042) to eliminate the excess PEG and to replace the original buffer of the BBI gold NPs with Millipore water. The final molar concentration of the solution was determined by UV/Vis spectroscopy using the extinction coefficient of the plain gold NPs. Gel electrophoresis was conducted by using 2% agarose gel (UltraPure, Invitrogen, Germany) under a constant voltage of 100 V for 50 min, which showed that the PEG-coated gold NPs have a small positive charge. Before particle exposure, the PEG-coated gold NPs were diluted with citrate buffer to a nominal concentration of 20 nM. The hydrodynamic diameter of the PEG-coated particles was estimated by gel electrophoresis to be around 25 nm.^[46]

Cell exposure and particle deposition: A recently developed exposure system was used for the air–liquid interface exposure of the cell cultures (ALICE) with the particles.^[30] The exposure procedure of gold NPs has previously been described.^[23,30] Briefly, micrometer-sized droplets were generated from the 20 nM particle suspension (1 mL) with a vibrating membrane droplet generator (investigational eFlow, PARI Pharma GmbH, Munich, Germany) and were deposited via cloud settling and single-particle sedimentation onto the cells in an exposure chamber. The NP deposition lasted 20 min followed by a particle exposure time of 1, 4, or 24 h. NP deposition and distribution at the air–liquid interface was analyzed as described previously^[23] and resulted in deposition of 16.1×10^9 (SD 1.5×10^9) citrate-stabilized gold particles cm⁻² and 14.1×10^9 (SD 1.6×10^9) PEG-coated particles cm⁻². It could also be shown that plain particles, which are only stabilized by citrate buffer and not by a PEG shell, were predominantly deposited onto the cells as single particles or small agglomerates (see the Supporting Information). Additional experiments were also performed to compare cellular NP deposition and uptake in the submerged exposure with those in the ALICE. The same number of plain particles as deposited on the cells per six-well insert (6.8×10^{10}) was dissolved in 1 mL cell culture medium (plain RPMI without FCS) and exposed to the cells for 4 h. The effects of diffusion and agglomeration of plain particles in suspension were subsequently analyzed and compared with the ALICE.

To investigate different endocytotic mechanisms of NP uptake, inhibition of caveolin- and clathrin-mediated endocytosis was performed with MβCD (Sigma Aldrich, Buchs, Switzerland).^[33] The cells were therefore incubated with 10 mM MβCD in phosphate-buffered saline for 30 min and washed with RPMI medium before the exposure. Each experiment was repeated three times.

Preparation for TEM: The cells on the insert membrane were fixed with 2.5% glutaraldehyde in 0.03 M potassium phosphate buffer for at least 24 h. The cells were then washed with buffer, post-fixed with 1% osmium tetroxide in sodium cacodylate buffer, washed with maleate, and stained en bloc with 0.5% uranyl acetate in maleate buffer. After additional washing, the cells were dehydrated in an ascending ethanol series, and embedded in epon.^[47] From the embedded cells, semi- and ultrathin sections were cut parallel to the vertical axis of the cells. Ultrathin sections were mounted on copper grids, stained with lead citrate and uranyl acetate, and were investigated with TEM.

Relative particle distribution within the cells: The method describing the RDI^[34] was designed to test whether intracellular NPs are localized randomly in all cellular compartments or if they

show any preferences for specific compartments. The observed particle density for each cellular compartment was estimated by relating the number of particle events in a given compartment to the corresponding fractional volume of the compartment.

All particle events (an event is defined as the intracellular occurrence of a single particle or agglomerate) were sampled by systematic uniform random sampling (reviewed in Reference [48]). This is fundamental for the acquisition of unbiased data in stereological image analysis. Details on sampling of particle events and sample preparations are given in the Supporting Information. Screening was performed on ultrathin TEM sections, with a Philips CM12 transmission electron microscope (FEI Co. Philips Electron Optics, Zürich, Switzerland) at a primary magnification of 25 000 \times . Each time a particle event was encountered, the cell compartment of its localization was reported and the largest diameter and the number of particles per particle event were recorded. Approximately 150 particle events were reported per experiment and the results of all three repetitions were pooled. The relative size of each cellular compartment was estimated by randomly superimposing a grid of test points over randomly located test fields (cells imaged at a magnification of 11 500 \times) and simply counting the number of points, $P(\text{comp})$, hitting each cellular compartment. More details on data acquisition are given in the Supporting Information.

The number of expected particles for each compartment, $N_E(\text{comp})$, assuming a purely random particle distribution within the cell, can be calculated from the total number of observed particles, $N_O(\text{total})$, and the numbers of observed points, $P(\text{total})$ and $P(\text{comp})$, by the following equation:

$$N_E(\text{comp}) = N_O(\text{total}) \frac{P(\text{comp})}{P(\text{total})} \quad (1)$$

From the observed $N_O(\text{comp})$ and expected $N_E(\text{comp})$ particle distributions, the RDI was calculated for each compartment:

$$\text{RDI} = \frac{N_O(\text{comp})}{N_E(\text{comp})} \quad (2)$$

An RDI > 1 indicates a preferentially populated compartment, that is, more NPs were found than expected for random intercellular NP distribution; an RDI < 1 represents a compartment that contains fewer NPs than expected solely from its size. An example of the calculation is given in Table 1. The observed and expected distributions were then statistically analyzed by the χ^2 test. A similar approach was used to compare observed distributions between two or more experimental groups, such as different time points, partial endocytotic inhibition, or different particle types. From the number of observed particles within each group, the number of expected particles was calculated for each compartment. This is the number of particles that would be expected if the distributions between the groups were equal. Again, the observed and the expected distributions of the different groups were statistically analyzed by the χ^2 test. If the total χ^2 value reached the significance level, the null hypothesis (“the particles are equally distributed among the cellular organelles” or “the intracellular particle distribution is equal among different experimental groups”) was rejected. A contribution of >10% of the

partial χ^2 value to the total χ^2 value indicated those compartments that contributed substantially to the nonrandom distribution or the intergroup differences, respectively.

Total particle uptake per cell: The total cellular NP uptake, with and without inhibition of clathrin- and caveolin-mediated endocytosis by M β CD treatment, was evaluated by quantifying the number of intracellular NPs. This was performed by estimating the intracellular particle density and multiplying the result by the average estimated cell volume. Particle events were counted for the distribution of the particles within the cells, whereas in this evaluation the total number of particles per cell was considered.

The intracellular particle density, N_V , defined as the ratio of the number of intracellular NPs per sampling volume, was estimated by applying an unbiased counting frame with defined test field area on TEM images obtained by systematic uniform random sampling (magnification 25 000 \times) and counting the number of NPs (N) in all test fields (n). An average number of 200–300 test fields per TEM section were evaluated with three independent sections per experiment and three repetitions per experimental condition (see systematic uniform random sampling in the Supporting Information). In this case, the total number of particles was counted, not the number of particle events. The volume was obtained by multiplying the test field area (A) by the section thickness (d), estimated by the method of the smallest fold,^[49] which is half of the diameter of the smallest fold in the ultrathin section (average section thickness: 50–80 nm).

$$N_V = \frac{N}{n A d} \quad (3)$$

For estimation of the mean cellular volume of cells, $\bar{V}_N(\text{cell})$, a number-weighted sampling procedure was used by application of the single-section disector. Thus, every time a nucleolus was observed in an A549 nucleus this cell was sampled for cell volume estimation by the vertical rotator.^[50] The rotator is a local stereological tool used to estimate the volume of a biological particle from a two-dimensional section. The sampling was performed on toluidene blue stained semithin sections with a conventional light microscope coupled to a CAST system (CAST 2.0, Olympus, Ballerup, Denmark) at an objective lens magnification of 60 \times . From these results the number-weighted mean cell volume, $\bar{V}_N(\text{cell})$, was estimated for each experiment. The average number of particles per cell, $\bar{N}(\text{cell})$, was obtained by:

$$\bar{N}(\text{cell}) = N_V \bar{V}_N(\text{cell}) \quad (4)$$

Statistics: To test if the intracellular particles were randomly distributed, the expected versus the counted particles were statistically analyzed with a χ^2 test and considered significant if the resulting χ^2 values exceeded the χ^2 values given in the tables of statistical analysis ($f=n-1$; $p \leq 0.05$). Furthermore, the intracellular particle distributions of different experimental setups, such as particle coating, incubation times, or partial inhibition of endocytosis, were also compared and analyzed with the χ^2 test.

The nonparametric Kruskal–Wallis One-Way Analysis of Variance (ANOVA) on Ranks was used to test if cellular particle uptake was reduced in M β CD-treated cells. If $p < 0.05$,

the Mann–Whitney *u*-test was further performed for comparison of two groups. Differences were considered significant at $p < 0.05$.

Acknowledgements

The authors would like to thank Mr. Bukalis and Mrs. Alber for performing the neutron-activated gamma spectroscopic determination of the mass of the gold nanoparticles and Barbara Krieger, Andrea Stokes, and Mohamed Ouanella for their excellent technical assistance, Kirsten Dobson for English proofreading, and Dr. Feng Zhang for the helpful discussions. This study was supported by grants of the Animal Free Research Foundation, the Doerenkamp-Zbinden Foundation, the Deutsche Forschungsgemeinschaft (DFG, SPP 1313), the Swiss National Science Foundation (3100Ao_118420), and the Helmholtz Association.

- [1] Y. Y. Liu, H. Miyoshi, M. Nakamura, *Int. J. Cancer* **2007**, *120*, 2527–2537.
- [2] J. Peteiro-Cartelle, M. Rodríguez-Pedreira, F. Zhang, P. Rivera Gil, L. del Mercato, W. J. Parak, *Nanomedicine* **2010**, *4*, 967–979.
- [3] S. Dhar, E. M. Reddy, A. Shiras, V. Pokharkar, B. L. Prasad, *Chem. Eur. J.* **2008**, *14*, 10244–10250.
- [4] H. M. Joshi, D. R. Bhumkar, K. Joshi, V. Pokharkar, M. Sastry, *Langmuir* **2006**, *22*, 300–305.
- [5] P. K. Jain, X. Huang, I. H. El-Sayed, M. A. El-Sayed, *Acc. Chem. Res.* **2008**, *41*, 1578–1586.
- [6] L. Olofsson, T. Rindzevicius, I. Pfeiffer, M. Kall, F. Hook, *Langmuir* **2003**, *19*, 10414–10419.
- [7] H. Hillaireau, P. Couvreur, *Cell. Mol. Life Sci.* **2009**, *66*, 2873–2896.
- [8] L. W. Zhang, J. Yang, A. R. Barron, N. A. Monteiro-Riviere, *Toxicol. Lett.* **2009**, *191*, 149–157.
- [9] J. Rejman, V. Oberle, I. S. Zuhorn, D. Hoekstra, *Biochem. J.* **2004**, *377*, 159–169.
- [10] K. Yin Win, S. S. Feng, *Biomaterials* **2005**, *26*, 2713–2722.
- [11] B. D. Chithrani, A. A. Ghazani, W. C. W. Chan, *Nano Lett.* **2006**, *6*, 662–668.
- [12] C. Brandenberger, B. Rothen-Rutishauser, F. Blank, P. Gehr, C. Mühlfeld, *Respir. Res.* **2009**, *10*, 22.
- [13] K. Unfried, C. Albrecht, L.-O. Klotz, A. Von Mikecz, S. Grether-Beck, R. P. F. Schins, *Nanotoxicology* **2007**, *1*, 52–71.
- [14] B. Rothen-Rutishauser, S. Schuerch, P. Gehr, in: *The Toxicology of Particles* (Eds: K. Donaldson, P. Borm), CRC, Boca Raton **2007**, pp. 139–160.
- [15] A. Lehmann, F. Zhang, Z. Ali, C. Röcker, G. U. Nienhaus, P. Gehr, B. Rothen-Rutishauser, *Small* **2010**, *6*, 753–762.
- [16] M. Geiser, M. Casaulta, B. Kupferschmid, H. Schulz, M. Semmler-Behnke, W. Kreyling, *Am. J. Respir. Cell. Mol. Biol.* **2008**, *38*, 371–376.
- [17] A. Verma, O. Uzun, Y. Hu, Y. Hu, H. S. Han, N. Watson, S. Chen, D. J. Irvine, F. Stellacci, *Nat. Mater.* **2008**, *7*, 588–595.
- [18] Y. J. Gu, J. Cheng, C. C. Lin, Y. W. Lam, S. H. Cheng, W. T. Wong, *Toxicol. Appl. Pharmacol.* **2009**, *237*, 196–204.
- [19] B. Rothen-Rutishauser, C. Mühlfeld, F. Blank, C. Musso, P. Gehr, *Part. Fibre Toxicol.* **2007**, *4*, 9.
- [20] H. J. Johnston, M. Semmler-Behnke, D. M. Brown, W. Kreyling, L. Tran, V. Stone, *Toxicol. Appl. Pharmacol.* **2010**, *242*, 66–78.
- [21] P. Nativo, I. A. Prior, M. Brust, *ACS Nano* **2008**, *2*, 1639–1644.
- [22] R. A. Sperling, P. Rivera Gil, F. Zhang, M. Zanella, W. J. Parak, *Chem. Soc. Rev.* **2008**, *37*, 1896–1908.
- [23] C. Brandenberger, B. Rothen-Rutishauser, C. Mühlfeld, O. Schmid, G. A. Ferron, K. L. Maier, P. Gehr, A. G. Lenz, *Toxicol. Appl. Pharmacol.* **2010**, *242*, 56–65.
- [24] Y. H. Chen, C. Y. Tsai, P. Y. Huang, M. Y. Chang, P. C. Cheng, C. H. Chou, D. H. Chen, C. R. Wang, A. L. Shiau, C. L. Wu, *Mol. Pharm.* **2007**, *4*, 713–722.
- [25] S. M. Ryan, G. Mantovani, X. X. Wang, D. M. Haddleton, D. J. Brayden, *Expert Opin. Drug Delivery* **2008**, *5*, 371–383.
- [26] A. Jain, S. K. Jain, *Crit. Rev. Ther. Drug Carrier Syst.* **2008**, *25*, 403–447.
- [27] S. D. Perrault, C. Walkey, T. Jennings, H. C. Fischer, W. C. W. Chan, *Nano Lett.* **2009**, *9*, 1909–1915.
- [28] Y. Zhang, N. Kohler, M. Zhang, *Biomaterials* **2002**, *23*, 1553–1561.
- [29] N. L. Rosi, D. A. Giljohann, C. S. Thaxton, A. K. R. Lytton-Jean, M. S. Han, C. A. Mirkin, *Science* **2006**, *312*, 1027–1030.
- [30] A. G. Lenz, E. Karg, B. Lentner, V. Dittrich, C. Brandenberger, B. Rothen-Rutishauser, H. Schulz, G. A. Ferron, O. Schmid, *Part. Fibre Toxicol.* **2009**, *6*, 32.
- [31] F. Blank, B. M. Rothen-Rutishauser, S. Schurch, P. Gehr, *J. Aerosol Med.* **2006**, *19*, 392–405.
- [32] L. K. Limbach, Y. Li, R. N. Grass, T. J. Brunner, M. A. Hintermann, M. Muller, D. Gunther, W. J. Stark, *Environ. Sci. Technol.* **2005**, *39*, 9370–9376.
- [33] S. K. Rodal, G. Skretting, O. Garred, F. Vilhardt, B. van Deurs, K. Sandvig, *Mol. Biol. Cell* **1999**, *10*, 961–974.
- [34] C. Mühlfeld, T. M. Mayhew, P. Gehr, B. Rothen-Rutishauser, *J. Aerosol Med.* **2007**, *20*, 395–407.
- [35] S. D. Conner, S. L. Schmid, *Nature* **2003**, *422*, 37–44.
- [36] D. Mandal, A. Maran, M. Yaszemski, M. Bolander, G. Sarkar, *Mater. Sci. Mater. Med.* **2009**, *20*, 347–350.
- [37] B. D. Chithrani, W. C. W. Chan, *Nano Lett.* **2007**, *7*, 1542–1550.
- [38] B. Ballou, B. C. Lagerholm, L. A. Ernst, M. P. Bruchez, A. S. Waggoner, *Bioconjugate Chem.* **2004**, *15*, 79–86.
- [39] C. Mühlfeld, P. Gehr, B. Rothen-Rutishauser, *Swiss Med. Wkly.* **2008**, *138*, 387–391.
- [40] R. Gref, M. Luck, P. Quellec, M. Marchand, E. Dellacherie, S. Harnisch, T. Blunk, R. H. Muller, *Colloids Surf. B Biointerfaces* **2000**, *18*, 301–313.
- [41] M. Lundqvist, J. Stigler, G. Elia, I. Lynch, T. Cedervall, K. A. Dawson, *Proc. Natl. Acad. Sci. USA* **2008**, *105*, 14265–14270.
- [42] C. Tekle, B. van Deurs, K. Sandvig, T. G. Iversen, *Nano Lett.* **2008**, *8*, 1858–1865.
- [43] M. A. Dobrovolskaia, A. K. Patri, J. Zheng, J. D. Clogston, N. Ayub, P. Aggarwal, B. W. Neun, J. B. Hall, S. E. McNeil, *Nanomedicine* **2009**, *5*, 106–117.
- [44] C. Röcker, M. Potzl, F. Zhang, W. J. Parak, G. U. Nienhaus, *Nat. Nanotechnol.* **2009**, *4*, 577–580.
- [45] M. S. Ehrenberg, A. E. Friedman, J. N. Finkelstein, G. Oberdörster, J. L. McGrath, *Biomaterials* **2009**, *30*, 603–610.
- [46] R. A. Sperling, T. Liedl, S. Dühr, S. Kuder, M. Zanella, C. A. J. Lin, W. H. Chang, D. Braun, W. J. Parak, *J. Phys. Chem. C* **2007**, *111*, 11552–11559.
- [47] C. Mühlfeld, B. Rothen-Rutishauser, D. Vanhecke, F. Blank, P. Gehr, M. Ochs, *Part. Fibre Toxicol.* **2007**, *4*, 11.
- [48] T. M. Mayhew, *Placenta* **2008**, *29*, 1–14.
- [49] J. V. Small, in *Proc. 4th European Regional Conf. Electron Microscopy* (Ed: D. S. Bocciarelli), Tipografia Poliglotta Vaticana, Rome **1968**, pp. 609–610.
- [50] E. B. V. Jensen, H. J. G. Gundersen, *J. Microsc.* **1993**, *170*, 282–282.

Received: April 1, 2010
Published online: